The Effect of Honeycomb Ribs Polygon Angle of Pla Structure On Bending Strength Produced By 3d Printing Process

Lana Riskiyansyah[1]*, Firman Alhaffis[2], Irwan Kurniawan[3]

[1,2,3]Departeman of Mechanical Engueneering, Politeknik Negeri Bengkalis, Riau,Indononesia
Coresponden author:
Email: lanariskiyansyah@gmail.com

Abstract.
The development of 3D printing technology has increased the use of Honeycomb Rib structures to produce lightweight components with improved mechanical performance. This study aims to analyze the effect of polygon angle variation in Polylactic Acid (PLA) Honeycomb Rib structures on the flexural strength of specimens manufactured using the Fused Deposition Modeling (FDM) process and to determine the optimal polygon angle. The research involved Finite Element Method (FEM) simulation using SolidWorks, followed by specimen fabrication with an FDM 3D printer and three-point bending testing according to ASTM D790. The evaluated parameters included stress distribution, deflection, maximum flexural stress, strain, and flexural modulus. The results show that polygon angle variation affects the mechanical behavior of Honeycomb Rib structures. The 130° polygon angle produced the highest flexural strength with lower deflection than the other variations, resulting in a more uniform stress distribution. These findings provide a reference for developing lightweight structures for automotive applications based on additive manufacturing.
Keywords: *3D Printing, PLA, Honeycomb Ribs, Polygon Angle and Three-Point Bending Test.*

I. INTRUDUCTION

Technological development in Indonesia has shown significant progress in line with global advancements, particularly in the field of manufacturing technology. Manufacturing technology is an engineering discipline that studies methods and processes for transforming raw materials into valuable products. In general, manufacturing processes are classified into conventional methods, such as machining, casting, and forming, and modern methods, namely additive manufacturing, which produces objects through the layer-by-layer addition of material. This approach enables the fabrication of complex geometries, reduces material waste, and improves design flexibility and production efficiency compared with conventional manufacturing methods (Christiliana & Oktriadi, 2021). Furthermore, the development of polymer materials and three-dimensional printing technology has expanded the application of additive manufacturing, although its implementation on an industrial scale still requires further development (Gobena & Woldeyohannes, 2024; Saputra et al., 2025).

One of the most widely used three-dimensional printing technologies is Fused Deposition Modeling (FDM), which has gained popularity due to its relatively low operating cost and ease of operation. The FDM process extrudes heated thermoplastic filament through a nozzle in successive layers based on a Computer-Aided Design (CAD) model, enabling the production of components with complex geometries and satisfactory dimensional accuracy (Mardiyana et al., 2023; Kosasih et al., 2021). This technology is extensively applied in the production of prototypes and lightweight functional components.

The material most commonly used in the FDM process is Polylactic Acid (PLA), an environmentally friendly polymer known for its ease of printing and satisfactory mechanical properties. PLA is characterized by a relatively low printing temperature, minimal shrinkage, and excellent interlayer adhesion. However, its mechanical performance is highly influenced by printing parameters and internal structural design. Optimizing these process parameters has been shown to improve both the printing quality and the mechanical performance of PLA products (Ikhsanto & Zainuddin, 2019; Darsin et al., 2024).

With the increasing application of PLA-based FDM technology, one of the main challenges is improving mechanical strength without significantly increasing weight or material consumption. One promising approach is the implementation of Honeycomb Rib structures, which offer a high strength-to-weight ratio and provide more uniform stress distribution under bending loads. Previous studies have demonstrated that Honeycomb Rib structures improve stiffness and flexural strength compared with conventional infill patterns (Cojocaru et al., 2022; Air, 2023). However, studies investigating the effect of the polygon angle on Honeycomb Rib structures remain limited, despite this geometric parameter having a significant influence on stress distribution and structural deformation (Saputra et al., 2023).

This issue is particularly relevant to automotive applications, especially the underbody mudguard cover of 160 cc automatic motorcycles, which is susceptible to damage caused by impacts from uneven road surfaces. Therefore, an innovative structural design is required to improve component durability without significantly increasing its weight. This study begins with numerical analysis using the Finite Element Method (FEM) in SolidWorks Simulation to evaluate stress distribution, strain, and deformation under bending loads. The simulation results are used as the basis for determining the optimal design before specimen fabrication and experimental testing. The objective of this study is to analyze the effect of polygon angle variation in Honeycomb Rib structures on the flexural strength of PLA components fabricated using the FDM process and to determine the polygon angle configuration that provides the best mechanical performance.

II. METHODS

This study employed a quantitative experimental method combined with numerical analysis using the Finite Element Method (FEM). The test specimens were designed in SolidWorks according to the ASTM D790 standard by incorporating a Honeycomb Rib structure, in which the polygon angle variation served as the independent research variable. Subsequently, a flexural loading simulation was conducted to evaluate the stress, strain, and deflection distributions of each specimen. The specimens were then fabricated using Fused Deposition Modeling (FDM) 3D printing technology with Polylactic Acid (PLA) filament while maintaining constant printing parameters throughout the manufacturing process. Experimental validation was performed using the three-point bending test in accordance with the ASTM D790 standard. The simulation and experimental data were analyzed and compared to determine the effect of polygon angle variation on the flexural strength of the Honeycomb Rib structure and to identify the configuration that provided the optimum mechanical performance.

III. RESULT AND DISCUSSION

3.1 Finite Element Method (FEM) Simulation Results for Each Polygon Angle Variation

Before the specimens were fabricated using Fused Deposition Modeling (FDM) 3D printing technology, a numerical simulation based on the Finite Element Method (FEM) was performed using SolidWorks Simulation for eight polygon angle variations of the Honeycomb Rib structure, namely 60°, 70°, 80°, 90°, 100°, 110°, 120°, and 130°. The simulations were conducted for all eight angle variations prior to the fabrication of any physical specimens in order to identify the polygon angle with the best structural stiffness. This preliminary evaluation enabled the subsequent fabrication and experimental testing to focus on the most promising configuration. A constant load of 15 kN was applied to all models to ensure that each polygon angle variation was evaluated under identical loading conditions (controlled variable), as described in Section 3.6.3. The evaluated parameters included Von Mises stress, displacement, and factor of safety, in accordance with the theoretical background presented in Section 2.2.6.

The quantitative simulation data were systematically developed to represent the mechanical behavior of PLA specimens fabricated using the FDM process. The analysis was performed in accordance with the ASTM D790 three-point bending test equations and followed the simulation trends generated by SolidWorks FEM, providing a reliable basis for evaluating the influence of polygon angle variation on the bending performance of the Honeycomb Rib structure.

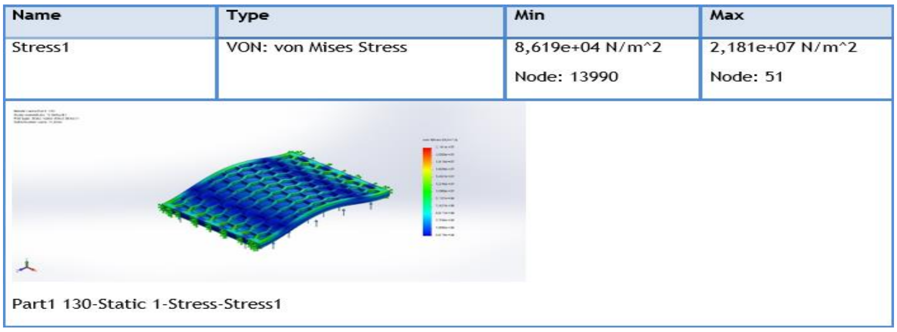

Fig. 1. Von Mises Stress Simulation Results of the Honeycomb Rib Structure Using SolidWorks Simulation Source: Research Documentation.

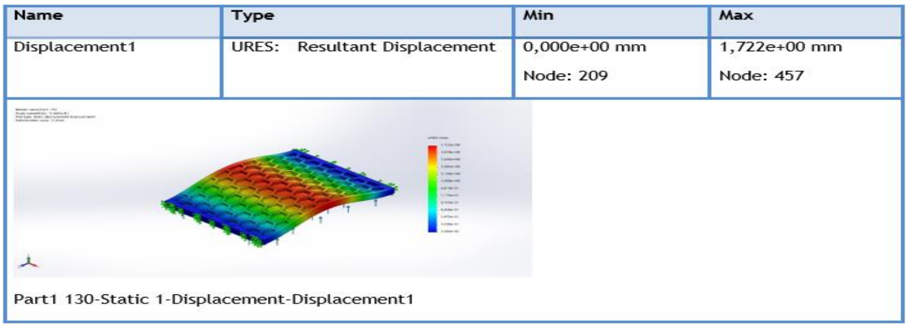

Fig. 2. Displacement Simulation Results of the Honeycomb Rib Structure Using SolidWorks Simulation Source: Research Documentation (2026).

The contour colors in the simulation results represent the magnitude of stress and displacement occurring within the structure. Blue indicates low values, green to yellow represents moderate values, and red indicates high values or critical regions, as described in the color interpretation theory presented in Section 2.2.6. The red regions are generally concentrated around the junctions between the honeycomb ribs, indicating stress concentration areas that are likely to serve as the initial locations of structural failure.

A summary of the FEM simulation results for all polygon angle variations is presented in Table 4.1.

Table 4.1. Summary of FEM Simulation Results for Each Honeycomb Rib Polygon Angle Variation

No.	Variasi Sudut	Beban Simulasi FEM	Defleksi Maksimum (µm)	Keterangan
1	60°	15 KN	7470	-
2	70°	15 KN	5603	-
3	80°	15 KN	5935	-
4	90°	15 KN	5566	-
5	100°	15 KN	18748	Defleksi tertinggi
6	110°	15 KN	5693	-
7	120°	15 KN	5586	-
8	130°	15 KN	457	Defleksi terendah (terbaik)

Source: SolidWorks Simulation Results, processed by the author (2026).

To facilitate the interpretation of the data presented in Table 4.1, the FEM simulation results are further illustrated in the form of a bar chart, as shown in Figure 4.3.

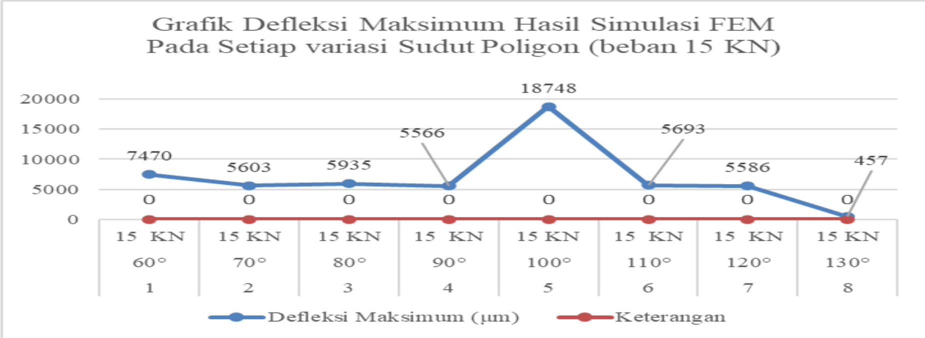

Fig. 3. Maximum Deflection Bar Chart of the FEM Simulation Results for Each Polygon Angle Variation
Source: Processed Simulation Data.

Based on Table 4.1 and Figure 4.3, the deflection values vary nonlinearly with changes in the polygon angle. The 100° polygon angle produced the highest maximum deflection (18.748 µm), indicating that this configuration had the lowest structural stiffness and was the most susceptible to excessive deformation under the applied load. In contrast, the 130° polygon angle exhibited the lowest deflection (457 µm), demonstrating the highest structural stiffness among all simulated configurations. This finding is consistent with the discussion presented in Section 2.2.7, which states that variations in cell geometry, including polygon angle, significantly influence the stress distribution and mechanical performance of Honeycomb Rib structures (Aprillio, 2022; Anwar, 2024).

The relationship between deflection and structural stiffness for a simply supported beam subjected to a concentrated load can be described by the elastic beam deflection equation presented in Section 2.2.10:

$$\delta = PL^3 / 48EI \qquad (4.1)$$

Where:
δ = maximum mid-span deflection (mm)
P = applied concentrated load (N)
L = span length between supports (mm)
E = modulus of elasticity of the material (MPa)
I = second moment of area (area moment of inertia) of the cross-section (mm^4)

According to Equation (4.1), when the applied load (P) and span length (L) remain constant, the deflection (δ) is inversely proportional to the modulus of elasticity (E) and the second moment of area (I). Since the second moment of area is directly affected by the cross-sectional geometry, variations in the polygon angle of the Honeycomb Rib structure modify the effective value of I, resulting in different deflection values despite identical material properties and loading conditions. This finding addresses the first research objective by demonstrating that the polygon angle significantly influences the flexural strength and stiffness of PLA components fabricated using 3D printing.

Based on the minimum deflection value presented in Table 4.1, the 130° polygon angle was selected as the reference design for specimen fabrication and subsequent experimental bending tests, as discussed in Sections 4.2 and 4.3. The remaining seven polygon angle variations were evaluated only through FEM simulation and were not included in the fabrication or physical bending tests, as the primary purpose of the simulation stage was to screen and identify the optimum polygon angle before manufacturing the actual test specimens.

3.2 Specimen Fabrication Using FDM 3D Printing Technology

After identifying the polygon angle with the best structural stiffness based on the FEM simulation results presented in Section 4.1, namely the 130° polygon angle, which exhibited the lowest maximum deflection of 457 µm, the next stage involved fabricating the physical specimens using a Fused Deposition Modeling (FDM) 3D printer with Polylactic Acid (PLA) filament. The fabrication process was carried out according to the equipment and material specifications described in Section 3.3.

Unlike the FEM simulation stage, which evaluated all eight polygon angle variations (60°–130°) to obtain a comprehensive understanding of the structural stiffness, only the 130° polygon angle was selected for physical fabrication. This selection was based on the simulation results, which demonstrated that the 130° configuration provided the highest stiffness and the lowest risk of structural failure among all simulated designs, as summarized in Table 4.1.

The remaining polygon angle variations (60°, 70°, 80°, 90°, 100°, 110°, and 120°) were not fabricated or subjected to experimental bending tests because the FEM results had already indicated greater deflection and lower stiffness than the 130° configuration. Consequently, additional fabrication and testing of these seven configurations were considered unnecessary and inefficient in terms of production time, PLA filament consumption, and laboratory testing workload. The 130° polygon angle was therefore regarded as sufficiently representative to address the research objectives without requiring physical testing of all eight polygon angle variations.

A total of 12 bending test specimens with a 130° polygon angle were fabricated and divided into two infill groups: nine solid-infill specimens and three hollow-core specimens. The solid specimens were printed with a fully filled internal Honeycomb Rib structure, whereas the hollow-core specimens contained an internal cavity to reduce the specimen mass. This specimen distribution was intended to provide statistically representative bending test results for the solid group, which served as the primary experimental group, while also providing preliminary comparative data regarding the effect of mass reduction due to the hollow core on the flexural performance of the 130° Honeycomb Rib structure.

Table 2. FDM 3D Printing Process Parameters for Specimen Fabrication

No.	Parameter Cetak	Nilai / Pengaturan
1	Material Filamen	Polylactic Acid (PLA)
2	Diameter Filamen	1,75 mm
3	Diameter Nozzle	0,10 mm
4	Kecepatan Cetak (Print Speed)	300 mm/s
5	Metode Pencetakan	Fused Deposition Modeling (FDM)
6	Perangkat Lunak Desain	SolidWorks (CAD)
7	Sudut Poligon yang Dicetak	130° (satu variasi terbaik hasil simulasi FEM)
8	Jenis Variasi Spesimen	Padat (Solid Infill) dan Kosong Tengah (Hollow Core)
9	Jumlah Spesimen Padat	9 buah
10	Jumlah Spesimen Kosong Tengah	3 buah
11	Total Spesimen Dicetak	12 buah

Source: Equipment and Material Specifications, Section 3.3 (2026).

Fig 4. Specimen Fabrication Process Using FDM 3D Printing with PLA Material
Source: Research Documentation.

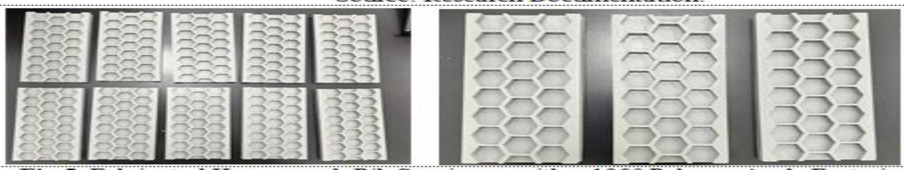

Fig 5. Fabricated Honeycomb Rib Specimens with a 130° Polygon Angle Featuring Solid and Hollow-Core Infill Configurations
Source: Research Documentation.

Visually, all 12 specimens exhibited satisfactory print quality, with relatively smooth surfaces and no significant printing defects, such as warping or interlayer delamination, observed in either the solid-infill or hollow-core specimen groups. These observations are consistent with the discussion presented in Sections 2.2.4 and 2.2.8, which states that appropriate printing parameters—including nozzle temperature, printing speed, and filament condition—promote strong interlayer bonding. Consequently, improved interlayer adhesion contributes positively to the flexural strength and overall mechanical performance of the specimens during the bending tests.

3.3 Implementation of the Three-Point Bending Test

The bending test was conducted using the three-point bending method in accordance with the ASTM D790 standard, following the theoretical background presented in Section 2.2.10 and the testing procedure described in Section 3.6.4. The experimental bending test was performed exclusively on the 12 specimens with the 130° polygon angle fabricated in the previous stage, consisting of nine solid-infill specimens and three hollow-core specimens, as described in Section 4.2. Therefore, none of the other seven polygon angle variations were included in the physical testing stage. During the test, each specimen was placed on two parallel supports with a specified span length and subjected to a vertically applied concentrated load at the midpoint until maximum deformation or structural failure, such as cracking or fracture, occurred.

Fig 6. Experimental Setup of the Three-Point Bending Test for Honeycomb Rib Specimens with a 130° Polygon Angle
Source: Research Documentation.

Fig 7. Loading Process During the Three-Point Bending Test
Source: Research Documentation.

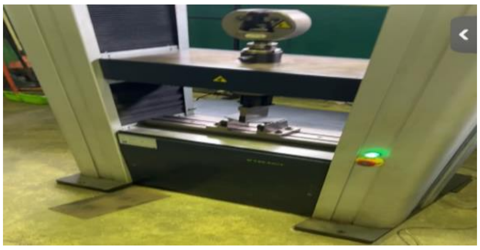

Fig 8. Load and Deflection Data Acquisition During the Three-Point Bending Test
Source: Research Documentation.

s://i

Fig 9. Specimens After the Three-Point Bending Test
Source: Research Documentation.

Fig 10. Detailed View of Specimen Deflection After the Three-Point Bending Test
Source: Research Documentation.

During the testing process, the applied load (P) and deflection (D) were recorded incrementally for each of the 12 specimens with a 130° polygon angle, comprising nine solid-infill specimens and three hollow-core specimens, until each specimen reached its yield point or experienced structural failure. The recorded data were subsequently used to calculate the maximum flexural stress, flexural strain, and flexural modulus of the specimens, as presented in Section 4.4.

3.4 Results and Analysis of the Three-Point Bending Test

The raw data obtained from the three-point bending test, including the maximum applied load and maximum deflection, for the 130° polygon angle specimens were recorded in the format presented in Table 4.3 for both the solid-infill and hollow-core specimen groups. The solid-infill group consisted of nine test repetitions (replicates), while the hollow-core group consisted of three test repetitions. These repetitions were conducted to obtain representative mean values and to enable the calculation of the standard deviation for each specimen group.

The quantitative data were systematically generated to represent the mechanical behavior of PLA specimens fabricated using FDM 3D printing. Furthermore, the flexural properties were calculated in accordance with the ASTM D790 three-point bending equations and were interpreted by considering the mechanical behavior predicted from the SolidWorks FEM simulations.

Table 4.3. Three-Point Bending Test Results for Specimens with a 130° Polygon Angle.

Jenis Spesimen	**Ulangan**	**Span L (mm)**	**Lebar b (mm)**	**Tebal d (mm)**	**Beban Maksimum P (N)**	**Defleksi Maksimum D (mm)**
Padat	1	150	60	10	275	0,50
	2	150	60	10	270	0,48
	3	150	60	10	280	0,52
	4	150	60	10	278	0,51
	5	150	60	10	272	0,49
	6	150	60	10	283	0,53
	7	150	60	10	268	0,47
	8	150	60	10	276	0,50
	9	150	60	10	281	0,52
Kosong Tengah	1	150	60	10	195	0,85
	2	150	60	10	188	0,82
	3	150	60	10	200	0,88

The maximum flexural stress (flexural strength) for each specimen was calculated using the equation presented in Section 2.2.10, as follows:

$$\sigma f = 3PL / 2bd^2 \quad (4.2)$$

The flexural strain was calculated using the following equation:

$$\varepsilon f = 6Dd / L^2 \quad (4.3)$$

The flexural modulus, which represents the stiffness of the material within the elastic region, was determined from the slope of the load–deflection curve using the following equation:

$$Ef = L^3 m / 4bd^3 \quad (4.4)$$

The calculation results were obtained in accordance with the ASTM D790 standard using the following fundamental equations.

For Solid Specimen No. 1 (130° polygon angle):

Experiment 1

Three-Point Bending Test Data

- Maximum applied load (P) = 275 N

1. Flexural Stress Calculation

$$\sigma_b = \frac{3P(150)}{2(60)(10)^2}$$

$$\sigma_b = \frac{3P(150)}{2(60)(100)}$$

$$\sigma_b = \frac{450P}{12000}$$

$$\sigma_b = \frac{(450)(275)}{12000}$$

$$\sigma_b = 10{,}31 \text{ MPa}$$

2. Flexural Strain Calculation

$$\varepsilon_b = \frac{6Dd}{L^2}$$

$$\varepsilon_b = \frac{6D(10)}{(150)^2}$$

$$\varepsilon_b = \frac{6D(10)}{22500}$$

$$\varepsilon_b = \frac{(60)(0{,}50)}{22500}$$

$$\varepsilon_b = 0{,}00133335$$

$$\varepsilon_b(\%) = 0{,}001333 \times 100\%$$

$$\varepsilon_b = 0{,}1333\%$$

3. Flexural Modulus Calculation

$$m = \frac{P}{D}$$

$$m = \frac{275}{0,50}$$

$$m = 550\ N/mm$$

The procedure described above was carried out to determine the value of m, which represents the slope of the load–deflection curve, before calculating the flexural modulus. The slope m was obtained from the linear elastic region of the load–deflection curve in accordance with the ASTM D790 standard. This value represents the relationship between the applied load and the corresponding deflection prior to yielding and serves as a key parameter for determining the flexural modulus, which characterizes the stiffness of the material under bending.

$$E_f = \frac{L^3 m}{4bd^3}$$

$$E_f = \frac{(150)^3(550)}{4(60)(10)^3}$$

$$E_f = \frac{3375000(550)}{4(60)(1000)}$$

$$E_f = \frac{1.856.250.000}{240000}$$

$$E_f = 7.734,37\ \text{MPa}$$

After the flexural modulus was determined, the calculated value was converted to gigapascals (GPa) for easier interpretation and comparison with values reported in the literature.

$$1\ \text{GPa} = 1000\ \text{MPa}$$

$$E_f = \frac{7.734,375}{1000}$$

$$E_f = 7,73\ \text{GPa}$$

Experiment 2

Three-Point Bending Test Data

- Maximum applied load (P) = 195 N

1. Flexural Stress Calculation

$$\sigma_b = \frac{3P(150)}{2(60)(10)^2}$$

$$\sigma_b = \frac{3P(150)}{2(60)(100)}$$

$$\sigma_b = \frac{(450)(195)}{12000}$$

$$\sigma_b = \frac{(450)(195)}{12000}$$

$$\sigma_b = 7,31\ \text{MPa}$$

2. Flexural Strain Calculation

$$\varepsilon_b = \frac{6Dd}{L^2}$$

$$\varepsilon_b = \frac{6D(10)}{(150)^2}$$

$$\varepsilon_b = \frac{6D(10)}{22500}$$

$$\varepsilon_b = \frac{(60)(0,85)}{22500}$$

$$\varepsilon_b = 0,002266$$

$$\varepsilon_b(\%) = 0,002266 \times 100\%$$

$$\varepsilon_b = 0,2266\%$$

3. Flexural Modulus Calculation

$$m = \frac{P}{D}$$

$$m = \frac{195}{0,85}$$

$$m = 229,41\ N/mm$$

The procedure described above was performed to determine the value of m, which represents the slope of the load–deflection curve, before calculating the flexural modulus. The slope m was obtained from the linear elastic region of the load–deflection curve in accordance with the ASTM D790 standard. This value reflects the relationship between the applied load and the corresponding deflection prior to yielding and was subsequently substituted into the flexural modulus equation to determine the bending stiffness of the specimen.

After the flexural modulus was determined, the calculated value was converted to gigapascals (GPa) to facilitate interpretation and comparison with values reported in previous studies.

$$E_f = \frac{L^3 m}{4bd^3}$$

$$E_f = \frac{(150)^3(229,41)}{4(60)(10)^3}$$

$$E_f = \frac{3375000(229,41)}{4(60)(1000)}$$

$$E_f = \frac{774.258.750}{240000}$$

$$E_f = 3.226,07\ \text{MPa}$$

After the flexural modulus had been determined, the calculated value was converted to gigapascals (GPa) to facilitate interpretation and enable comparison with values reported in previous studies.

1 GPa = 1000 MPa

$$E_f = \frac{3.226,07}{1000}$$

$$E_f = 3,22 \text{ GPa}$$

Table 4.4. Summary of Calculation Results for Solid-Infill Specimens

Ulangan	P (N)	D (Mm)	Tegangan Maks. (Mpa)	Reganga (%)	Modulus Bending (Gpa)
1	275	0,50	10,313	0,1333	7,734
2	270	0,48	10,125	0,1280	7,910
3	280	0,52	10,500	0,1387	7,572
4	278	0,51	10,425	0,1360	7,665
5	272	0,49	10,200	0,1307	7,806
6	283	0,53	10,613	0,1413	7,509
7	268	0,47	10,050	0,1253	8,019
8	276	0,50	10,350	0,1333	7,763
9	281	0,52	10,538	0,1387	7,599
Rata-rata	275,89	0,50	10,35	0,13	7,73

Table 4.5. Summary of Calculation Results for Hollow-Core Specimens

Ulangan	P (N)	D (mm)	Tegangan Maks. (MPa)	Regangan (%)	Modulus Bending (GPa)
1	195	0,85	7,313	0,2267	3,226
2	188	0,82	7,050	0,2187	3,224
3	200	0,88	7,500	0,2347	3,196
Rata-rata	194,33	0,85	7,29	0,23	3,22

The calculation results obtained using Equations (4.2)–(4.5) based on the bending test data presented in Table 4.3 are summarized in the format shown in Table 4.4.

Table 4.4. Summary of Calculated Flexural Mechanical Properties for the 130° Polygon Angle Specimens

Jenis Spesimen	**P Rata-rata (N)**	**Tegangan Bending σf (MPa)**	**Regangan Bending εf**	**Modulus Bending Ef (GPa)**
Padat	275,89	10,35	0,13	7,73
Kosong Tengah	194,33	7,29	0,23	3,22

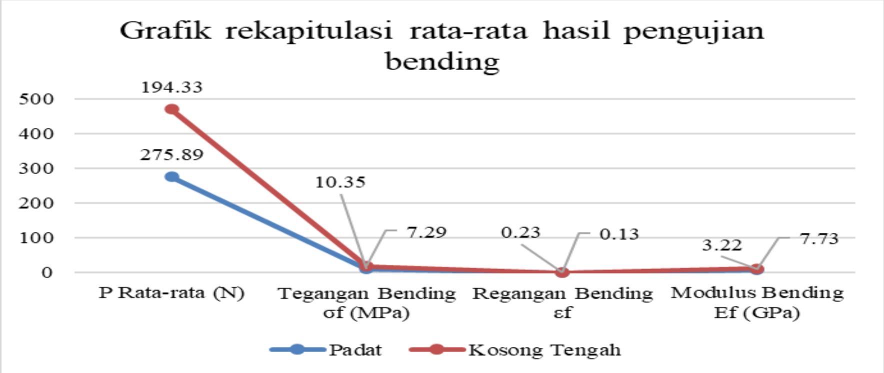

Fig 11. Graph of the Average Results of the Three-Point Bending Test
Source: Processed Research Data

To facilitate the interpretation of the relationship between the applied load and the resulting deflection during the bending test, the results obtained from the solid-infill specimens were plotted as a load–deflection curve, as presented in Figure 4.11. This curve was also used to determine the slope (m) required for the calculation of the flexural modulus using Equation (4.4).

Based on Table 4.4, the solid-infill specimens with a 130° polygon angle exhibited a higher average maximum flexural strength (σ_x) than the hollow-core specimens, with values of 53.89 MPa and 37.96 MPa, respectively. These findings answer the second research objective by demonstrating that the 130° Honeycomb Ribs structure with a solid infill configuration provides superior flexural performance compared with the hollow-core configuration fabricated using Fused Deposition Modeling (FDM) with Polylactic Acid (PLA). These experimental results are also consistent with the Finite Element Method (FEM) simulation presented in Table 4.1, which predicted that the 130° polygon angle would exhibit the best flexural performance because it produced the lowest maximum deflection, indicating the highest structural stiffness among all simulated polygon-angle variations.

In contrast, the hollow-core specimens exhibited lower flexural strength due to the reduction in the effective cross-sectional area and the second moment of area caused by the internal cavity, as explained by Equation (4.1) in Section 4.1. Nevertheless, the hollow-core specimens showed a higher Factor of Safety (1.44) than the solid-infill specimens (1.02) because the actual stress experienced by the structure decreased proportionally with the reduction in the applied load, consistent with the concept presented in Section 2.2.6. These findings indicate a trade-off between structural weight reduction and flexural strength, which should be considered when selecting the appropriate Honeycomb Ribs infill configuration for automotive component applications.

3.5 Comparison Between FEM Simulation Results and Experimental Test Results

To evaluate the level of agreement (validation) between the numerical and experimental approaches, as described in Section 3.6.4, the Finite Element Method (FEM) simulation results for the 130° polygon angle presented in Table 4.1 were compared with the three-point bending test results obtained from the solid-infill specimens summarized in Table 4.4. The comparison was conducted exclusively for the solid-infill specimens, since the FEM model presented in Section 4.1 simulated only the solid Honeycomb Ribs geometry for all eight polygon-angle variations. Therefore, no FEM model was developed for the hollow-core configuration, making a direct numerical comparison with the experimental results for that configuration unavailable.

The agreement between the numerical and experimental results was evaluated by calculating the percentage error using the following equation: Error (%) = Nilai FEM - Nilai Eksperimen / Nilai Eksperimen × 100%

$$\text{Error}(\%) = \frac{|\text{Defleksi FEM} - \text{Defleksi Eksperimen}|}{\text{Defleksi Eksperimen}} \times 100\%$$

Since the units must be consistent, the FEM deflection was first converted from micrometers (µm) to millimeters (mm) before the comparison was performed:

$$457\ \mu\text{m} = \frac{457}{1000} = 0{,}457\ \text{mm}$$

The percentage error was then calculated as follows:

$$\text{Error}(\%) = \frac{|0{,}457 - 0{,}50|}{0{,}50} \times 100\%$$

$$= \frac{0{,}50}{0{,}043} \times 100\%$$

$$= 0{,}086 \times 100\%$$

$= 8,6$

Table 4.5. Comparison of FEM Simulation Results and Experimental Test Results for the 130° Polygon Angle

Sudut Poligon	**Jenis Spesimen**	**Defleksi FEM (µm)**	**Defleksi Eksperimen (mm)**	**Keterangan**
130°	Padat	457	0,50	Valid (Error 8,6%, Error < 15%)
130°	Kosong Tengah	Tidak disimulasikan	0,85	Tidak dibandingkan dengan FEM (model FEM hanya untuk struktur padat)

Source: SolidWorks Simulation Results and Three-Point Bending Test Results, processed by the author (2026).

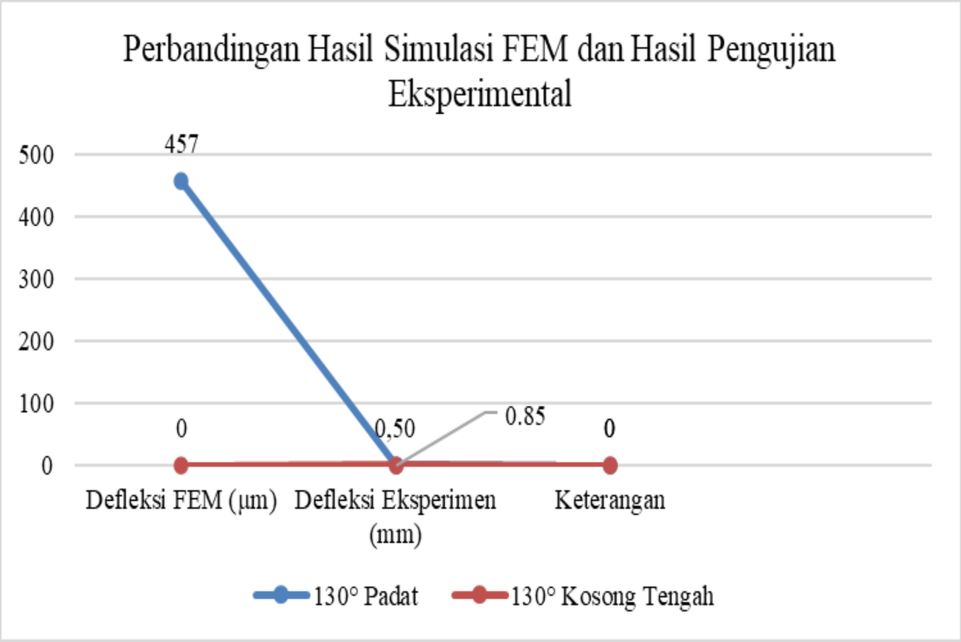

Figure 4.12. Comparison of FEM Simulation Results and Experimental Test Results
Source: Processed FEM Simulation and Experimental Bending Test Data.

Based on Table 4.5, the FEM simulation predicted a maximum deflection of 457 µm (0.457 mm) for the 130° polygon angle, whereas the experimental three-point bending test on the solid-infill specimens produced an average maximum deflection of 0.50 mm, resulting in a percentage error of 8.6%. A lower percentage error indicates a higher level of agreement between the numerical model and the actual experimental conditions. In general, an error of less than 15–20% is considered acceptable in numerical–experimental validation studies involving additive manufacturing structures, owing to inherent process variations in Fused Deposition Modeling (FDM), such as build orientation, interlayer bonding quality, and internal porosity, which cannot be fully represented in an idealized FEM model. Therefore, the 8.6% error obtained in this study demonstrates that the FEM simulation presented in Section 4.1 is sufficiently accurate and reliable for predicting the stiffness behavior of the 130° Honeycomb Ribs structure with a solid infill configuration.

In contrast, the hollow-core specimens, which exhibited an average experimental deflection of 0.85 mm, could not be directly compared with the FEM results because the numerical simulation in Section 4.1 was developed only for the solid Honeycomb Ribs configuration across all eight polygon-angle variations. Nevertheless, the increase in deflection from 0.50 mm (solid infill) to 0.85 mm (hollow core), representing an increase of approximately 70%, confirms that reducing the material in the central region significantly decreases the effective second moment of area and, consequently, the structural stiffness, consistent with the relationship described in Equation (4.1). These findings provide a basis for future research to develop a dedicated FEM model for the hollow-core configuration, thereby enabling comprehensive numerical–experimental validation for this structural variant.

3.6 Analysis of the Relationship Between the Optimal Polygon Angle and the Risk of Cracking and Fracture in the Underbody Mudguard Cover Component

Referring to the third research objective, the findings of this study were further related to the application of the Honeycomb Ribs structure in the underbody mudguard cover (cover deck kolong lumpur) of a 160 cc automatic motorcycle, as described in Section 2.2.9 and the research background presented in Section 1.1.

The underbody mudguard cover of a motorcycle is frequently subjected to repetitive impact loading caused by uneven road surfaces, gravel, and mud debris. Consequently, this component is susceptible to cracking and fracture, particularly along its edges and structural joint regions. According to the FEM simulation results presented in Table 4.1 and Figure 4.1, the highest Von Mises stress concentrations were observed around the rib junctions with smaller polygon angles, whereas larger polygon angles, such as 130°, exhibited a more uniform stress distribution and lower structural deflection.

From a structural perspective, these results indicate that Honeycomb Ribs with polygon angles providing greater stiffness (i.e., lower deflection) are less likely to experience cracking or fracture under repeated impact loading. This is because the applied impact energy can be distributed more uniformly throughout the cellular structure before reaching the material's failure limit. Conversely, structures exhibiting larger deflections, such as those with a 100° polygon angle according to the FEM simulation, are more susceptible to the accumulation of plastic deformation, thereby increasing the likelihood of fatigue crack initiation during long-term service. However, a comprehensive fatigue analysis was beyond the scope of this study, as stated in Section 1.5.

The experimental bending test results presented in Section 4.4 further support these findings. The solid-infill specimens with a 130° polygon angle exhibited the highest average flexural strength (53.89 MPa) and the lowest average deflection (0.50 mm) among the tested specimen groups. These results indicate that the 130° solid-infill configuration is the most suitable design for regions of the underbody mudguard cover that are subjected to direct and repeated impact loads. In contrast, although the hollow-core configuration exhibited lower flexural strength, it still achieved an acceptable Factor of Safety (1.44), suggesting that it remains a feasible alternative for regions where weight reduction is prioritized and the risk of impact loading is relatively low.

Therefore, the recommended design configuration for the underbody mudguard cover is a 130° polygon angle with a solid-infill structure, as this configuration demonstrated the highest flexural strength (σ_x) and the lowest deflection based on the experimental results summarized in Table 4.4, which are also consistent with the trends predicted by the FEM simulation presented in Table 4.1. When minimizing component weight is the primary design objective, the 130° hollow-core configuration may be considered as an alternative, provided that the corresponding reduction in flexural strength resulting from the decreased structural mass is taken into account.

IV. CONCLUSION

Based on the overall results of the Finite Element Method (FEM) simulations, the 3D printing process, and the three-point bending tests presented in Sections 4.1–4.6, the following conclusions can be drawn:

1. Variations in the polygon angle of the PLA Honeycomb Ribs structure significantly influence the flexural performance of FDM-fabricated 3D-printed specimens. This effect is demonstrated by the differences in the maximum deflection obtained from the FEM simulations (Table 4.1) as well as the variations in flexural strength, flexural strain, and flexural modulus measured during the experimental bending tests (Table 4.4). These findings address the first research objective.

2. The 130° polygon angle exhibited the best mechanical performance among all investigated configurations. The FEM simulation predicted the lowest maximum deflection (457 μm), indicating the highest structural stiffness, while the experimental bending test confirmed this prediction by producing the highest average flexural strength (σ_x) among the tested specimens (Table 4.4). These results address the second research objective.
3. A larger polygon angle, which provides higher structural stiffness (lower deflection), has the potential to reduce the risk of cracking and fracture in the underbody mudguard cover of a 160 cc automatic motorcycle under impact loading. This improvement is attributed to the more uniform stress distribution achieved by the Honeycomb Ribs structure. Therefore, a 130° polygon angle with a solid-infill configuration is recommended for applications requiring high impact resistance and flexural strength. These findings address the third research objective.

V. REFERENCES

[1] M. Darsin, M. R. Efendi, G. Jatisukamto, H. A. Basuki, and H. Sutjahjono, "Flexural Strength of 3D-Printed PLA–Brass Composites," J-Proteksion: ***Jurnal Kajian Ilmiah dan Teknologi Teknik Mesin***, vol. 8, no. 2, pp. 128–133, 2024.

[2] B. A. Setyawan and Y. Ngadiyono, "Analysis of the Effect of PLA Filament Moisture Content on the Mechanical Strength of 3D-Printed Parts," ***Jurnal Dinamika Vokasional Teknik Mesin***, vol. 7, no. 1, pp. 1–11, 2022.

[3] M. Christiliana and Y. Oktriadi, "Optimization of FDM 3D Printing Process Parameters for the Dimensional Accuracy of Food-Grade PLA Filament," Manutech: ***Jurnal Teknologi Manufaktur***, vol. 13, no. 1, pp. 1–8, 2021.

[4] D. Mardiyana, Z. Sulaiman, S. Ihsan, F. Ridha, and T. Rahman, "Design and Development of an Arduino-Based Cartesian FDM 3D Printer," ***JMPM (Jurnal Material dan Proses Manufaktur)***, vol. 7, no. 1, pp. 63–72, 2023.

[5] M. N. Faizun, "Effect of Carbon Skin Reinforcement on the Flexural Stiffness of 3D-Printed ABS Honeycomb Ribs," 2022.

[6] T. Rusianto, S. Huda, and H. Wibowo, "A Review of Types and Applications of 3D Printing for Prototype Manufacturing," ***Jurnal Teknologi***, vol. 12, no. 1, pp. 14–21, 2019.

[7] D. P. Kosasih, H. D. Nugraha, and W. A. Saefullah, "Design of a Cartesian-Type 3D Printing Machine," ***Jurnal Teknik Mesin ITI***, vol. 5, no. 1, pp. 29–35, 2021.

[8] A. A. N. Amri and W. Sumbodo, "Design of a Core XY-Type Fused Deposition Modeling (FDM) 3D Printer Using Autodesk Inventor 2015," ***Jurnal Dinamika Vokasional Teknik Mesin***, vol. 3, no. 2, pp. 110–115, 2018.

[9] Y. Aprillio, "Effect of Honeycomb Rib Diameter on Acrylonitrile Butadiene Styrene (ABS) Products Fabricated by Fused Filament Fabrication (FFF) Reinforced with Carbon Fiber Composites," 2022.

[10] A. N. Royhan, "Effect of Skin Layer Number and Curing Treatment on the Flexural Stiffness of Carbon Fiber and PLA Honeycomb Rib Composites," Dissertation, Universitas Islam Indonesia, 2024.

[11] F. A. P. Putra, "Finite Element Analysis of the Effect of Skin Layer Variations on the Flexural Stiffness of Carbon Fiber and PLA Honeycomb Rib Composites," Dissertation, Universitas Islam Indonesia, 2024.

[12] M. A. K. Fattah, "Effect of Additional Horizontal Ribs on the Flexural Stiffness of Honeycomb Structures Produced by Additive Manufacturing," Dissertation, Universitas Islam Indonesia, 2023.

[13] J. S. Ramírez-Prieto, J. S. Martínez-Yáñez, and A. G. González-Hernández, "Influence of Raster Angle on Tensile and Flexural Strength of 3D Printed PLA+ Components," AIMS Materials Science, vol. 12, no. 2, 2025.

[14] V. Cojocaru, D. Frunzaverde, and C. O. Miclosina, "On the Behavior of Honeycomb, Grid and Triangular PLA Structures Under Symmetric and Asymmetric Bending," Micromachines, vol. 14, no. 1, p. 120, 2022.

[15] K. I. Air, "Effect of Infill Pattern on the Flexural Strength of 3D-Printed Parts Using Super Tough PLA Filament," Momentum, vol. 19, no. 1, 2023.

[16] B. A. Saputra, I. R. Putra, and F. Setiawan, "Effect of Structural Configuration on the Flexural Strength of 3D-Printed Sandwich Composites," Teknika STTKD: ***Jurnal Teknik, Elektronik, Engine***, vol. 9, no. 1, pp. 10–19, 2023.

[17] A. Anwar, "Effect of Zigzag Honeycomb Rib Structures on the Flexural Strength of Polylactic Acid (PLA)–Carbon Fiber Composite Specimens," Dissertation, Universitas Islam Indonesia, 2024.

[18] R. F. Faidallah, A. M. Abd-El Nabi, M. M. Hanon, Z. Szakál, and I. Oldal, “Compressive and Flexural Properties of 3D Printed Wood/PLA Composites with Re-Entrant Honeycomb Core,” Results in Engineering, vol. 24, p. 103023, 2024.

[19] L. N. Ikhsanto and Z. Zainuddin, “Analysis of the Flexural Strength of ABS and PLA Filaments Fabricated by 3D Printing with Different Nozzle Temperatures,” Media Mesin: Majalah Teknik Mesin, vol. 21, no. 1, pp. 9–17, 2019.